Oceanic El-Niño wave dynamics and climate networks

2016 New J. Phys. 18 033021

(http://iopscience.iop.org/1367-2630/18/3/033021)

New Journal of Physics
The open access journal at the forefront of physics

Deutsche Physikalische Gesellschaft DPG
IOP Institute of Physics

Published in partnership with: Deutsche Physikalische Gesellschaft and the Institute of Physics

OPEN ACCESS

RECEIVED
1 October 2015

REVISED
13 January 2016

ACCEPTED FOR PUBLICATION
17 February 2016

PUBLISHED
11 March 2016

PAPER

Oceanic El-Niño wave dynamics and climate networks

Yang Wang[1], **Avi Gozolchiani**[2], **Yosef Ashkenazy**[2] **and Shlomo Havlin**[1]

[1] Department of Physics, Bar-Ilan University, Ramat-Gan 52900, Israel
[2] Solar Energy and Environmental Physics, Blaustein Institutes for Desert Research, Ben-Gurion University of the Negev, Israel

E-mail: wangyang.maple@gmail.com

Keywords: El-Niño, complex networks, climate networks, complex systems, fluid dynamics

Abstract

The so-called El Niño-southern oscillation (ENSO) is the most important and influential climate phenomenon of contemporary climate variability, in which oceanic wave dynamics plays an important role. Here we develop and apply an approach based on network theory to quantify the characteristics of El-Niño related oceanic waves using the satellite dataset. We associate the majority of dominant long distance ($\geqslant$500 km) links of the network with several kinds of oceanic waves, i.e. equatorial Kelvin, Rossby, and tropical instability waves. Notably, we find that the location of the out-going ($\sim$180°E) and in-coming hubs ($\sim$140°W) of the climate network coincide with the locations of the wave initiation and dissipation, respectively. We also find that this dissipation at $\sim$140°W is much weaker during El-Niño times. Moreover, the hubs of the equatorial network agree with the locations of westerly wind burst activity and high wind vorticity, two mechanisms that were associated with Rossby waves activity. This novel quantification method that is directly based on observational data leads to a better understanding of the oceanic wave dynamics, and it can also improve our understanding of El-Niño dynamics or its prediction.

1. Introduction

The El Niño-southern oscillation (ENSO) is the largest climatic cycle on annual time scales, and is one of the most important processes that affect the natural climate variability. During El-Niño (which occurs every 2–7 years) the eastern Pacific ocean becomes warmer by a few degrees and, the pressure in the east (west) Pacific is low (high) compared with normal times, leading to weaker easterly (coming from the east) winds. El-Niño is often accompanied by heavy floods in the South American countries and severe droughts in some other countries including Australia and Indonesia. It has been shown that El-Niño has a profound effect not only on the tropical atmospheric and oceanic conditions, but also on remote regions including North America, Indian monsoon region, and Antarctica [1–3]. Classical theories of El-Niño attribute its self-sustained dynamics mainly to positive and negative feedbacks between the depth of the thermocline, internal Kelvin and Rossby waves, sea-surface temperature (SST), and winds.

Changes in the climate variables such as SST, pressure, and wind strength affect the upper ocean that responds to the atmosphere. This atmosphere-ocean feedback is associated with internal waves in the upper ocean. Oceanic wave dynamics plays an important role in El-Niño dynamics, and the equatorial region can be regarded as a natural waveguide of several degree latitude width centered at the equator [4]. The most important El-Niño waves are the equatorial Kelvin waves and long equatorial Rossby waves, that travel at the upper ocean (tens of meters below the surface at the eastern Pacific to a few hundreds of meters at the western Pacific). The equatorial Kelvin waves travel to the east, and can cross the Pacific basin in about $\sim$2.5 months. Long equatorial Rossby waves travel to the west, crossing the Pacific basin in about 7 months. Briefly (and simplistically), the weakening of winds at the central Pacific initiates downwelling Kelvin waves and long Rossby waves. The Kelvin waves travel eastward and warm the eastern Pacific, resulting in El-Niño . At the same time downwelling long Rossby waves slowly propagate to the west, 'collide' with the western boundary of the Pacific ocean, and reflected

back as upwelling Kelvin waves. These reflected Kelvin waves cool the eastern Pacific ocean—when they reach the eastern Pacific after about ten months they terminate the El-Niño .

The intraseasonal Kelvin waves have been extensively studied using various observational and modeling methods due of their importance to the theory of El-Niño [5]. For example, the 1997/8 strong El-Niño event was initiated by a group of very pronounced Kelvin waves which were generated by energetic westerly wind bursts (WWBs) [6]. Recently, satellite altimetry data has become an invaluable resource to study equatorial wave dynamics [7, 8]. The velocity of waves in the equatorial Pacific region can be estimated using the so-called Hovmöller (longitude-time) diagrams, by transferring the data to the wavenumber-frequency space, or by decomposing the data into several leading modes of equatorial Kelvin and Rossby waves [8, 9]. Generally speaking, the typical phase speeds of the first baroclinic mode of equatorial Kelvin and Rossby waves are $\sim$2.8 m s^{-1} and $\sim$0.9 m s^{-1}, respectively [8, 9] where Kelvin waves exist on the equator and propagate eastward while Rossby waves are propagating to the west.

Tropical oceanic waves connect different, sometimes very far, regions. The set of regions V and their interactions E can be encoded in a graph $G(V, E)$ named in recent literature 'climate network' [10]. Many fields of research benefit from a rich set of quantifications and algorithms that has been developed for analyzing such networks of interactions. Examples include social and biological systems, information flow through the world wide web and physiological activities (see [11, 12] for reviews). In climate science, network theory has been used, e.g., to infer known climate patterns (like ocean currents), to investigate atmospheric variabilities, and to study low-frequency climate phenomena [10, 13–20]. It is common to regard links from E whose statistical significance is above a certain threshold as weighted or unweighted links. Since network based methods emphasize coordination between locations rather than local dynamics, they exhibit an increased sensitivity to climate patterns which are not easily captured by conventional analysis [17, 19]. In spite of the importance of oceanic dynamics on the climate system, only a few studies have used oceanic data within the framework of climate networks [19, 21]. Also, the studies of El-Niño using climate network methodology took advantage of near surface atmospheric data [13, 17, 18]. Here we aim to fill this gap based on the observational oceanic data, focusing on the important ocean-atmosphere phenomenon, El-Niño.

By transforming the daily and relatively long ($\sim$20 years) satellite based altimeter (i.e., sea surface height (SSH)) records into climate networks using cross correlation, we find that the time delays, the velocities and the directions associated with climate network links can be attributed to equatorial Kelvin, Rossby and tropical instability waves (TIWs). As will be shown below, the topology of the climate network is strongly affected by El-Niño, which implies that the relative number of links in the eastern equatorial Pacific is significantly higher during El-Niño times compared to normal times. Notably, the network properties (i.e. degree distribution) reveal the locations of the wave initiation as well as its strong dissipation. We note that the developed climate network approach leads us to better understand several new aspects of El-Niño related oceanic wave properties including the concentration of the waves in specific regions/specific times, and the decay location of the Kelvin waves ($\sim$120°W). In contrast to previous related work that relied on model's simulations [22], all of our results are based only on observational data. Note that recent studies have developed methods to uncover the direct and indirect connections in the climate network [23–25]. Distinguishing them is not the focus of our current study and we hope to address the question of direct versus indirect links in the near future.

2. Methodology

We analyze the daily SSH anomaly data[3]. We focus on the tropical Pacific ocean between 7°S and 7°N, and between 120°E and 280°E (80°W); the time extent of the data is from 1 January 1993 to 31 December 2010. The spatial resolution is 1° and 4° in the meridional and zonal directions, respectively. Totally, there are 615 grid points, which are regarded as nodes of the climate network. For each node of the network, we analyze daily SSH values after subtracting the seasonal cycle. The filtered SSH record is denoted by H. We also define the normalized series $\Theta_s(t) \equiv [H_s(t) - \langle H_s(t)\rangle]/\langle (H_s(t) - \langle H_s(t)\rangle)^2\rangle^{1/2}$, where $\langle\cdots\rangle$ represents the temporal average, s is the location, and t is the time parameter.

A link between each pair of sites s_1 and s_2 on year y is defined based on the lagged cross-correlation function $X^y_{s_1,s_2}(\tau \geqslant 0) = \langle \Theta^y_{s_1}(t)\Theta^y_{s_2}(t+\tau)\rangle$, and $X^y_{s_1,s_2}(\tau) = X^y_{s_2,s_1}(-\tau)$, where τ is the time lag parameter that is considered up to 200 d (the results are not sensitive to this parameter). We also define the optimal time lag, τ^*, at which $X^y_{s_1,s_2}(\tau)$ is maximal (or minimal), as the time delay of a pair s_1, s_2. When s_1 is to the west of s_2 and the time lag is positive, the link direction is to the east. We distinguish between positive and negative link *weights* as follows

[3] The Ssalto/Duacs altimeter products were produced and distributed by the Copernicus Marine and Environment Monitoring Service (CMEMS) (http://www.marine.copernicus.eu).

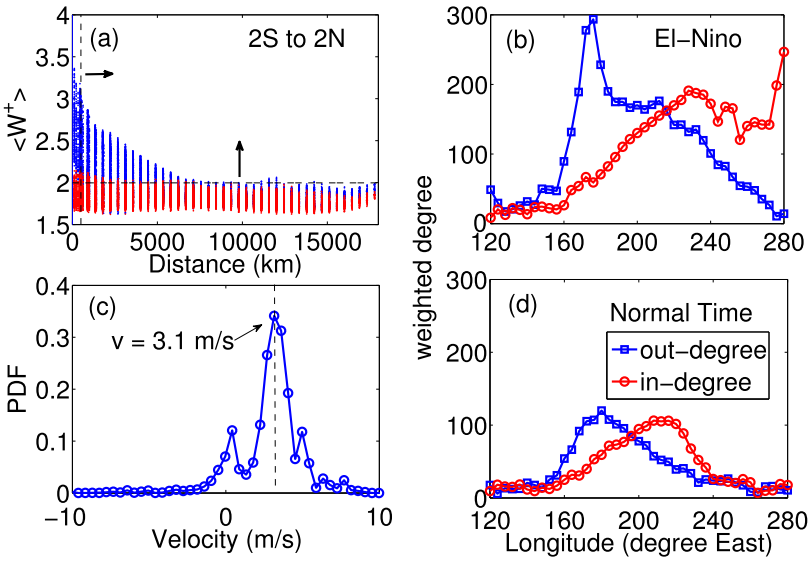

Figure 1. Equatorial Pacific network (2°N–2°S) analysis. (a) The temporal mean weight of positive links $\langle W^{+}\rangle$ versus their distance for both real (blue dots) and shuffled (red dots) data. (b) The 'in' (red circles) and 'out' (blue squares) weighted degree as a function of longitude for El-Niño times, for positive links ($p \leqslant 0.02$ and $D \geqslant 500$ km). (c) The probability density function (PDF) of phase speeds that are based on positive links with $p \leqslant 0.02$ and distances larger than 500 km. (d) Same as (b) but for normal times.

$$W^{y,+}_{s_1,s_2} = \frac{\max(X^{y}_{s_1,s_2}) - \mathrm{mean}(X^{y}_{s_1,s_2})}{\mathrm{std}(X^{y}_{s_1,s_2})}, \tag{1}$$

and

$$W^{y,-}_{s_1,s_2} = \frac{\min(X^{y}_{s_1,s_2}) - \mathrm{mean}(X^{y}_{s_1,s_2})}{\mathrm{std}(X^{y}_{s_1,s_2})}, \tag{2}$$

where max and min are the maximum and minimum values of the cross-correlation $X^{y}_{s_1,s_2}(\tau)$, mean and std represents the mean and standard deviation. Each climate network is constructed based on 1 yr SSH data, and the time resolution for two consecutive climate network is 30 d. To eliminate the effect of slow modulations on correlation estimates, a two years high-pass filter has been used. Examples of SSH time series and their cross correlation-function is presented in figure A1 of appendix A.

3. Results

3.1. Equatorial Pacific

We construct climate networks for three sub-regions of the tropical Pacific: equatorial Pacific (2°S–2°N), northern tropical Pacific (4°N–7°N) and southern tropical Pacific (4°S–7°S). To identify a threshold below which link weights W can be disregarded, we apply a shuffling procedure in which the order of calendar years is shuffled while the order of days within each year remains unchanged. Thus, the statistical properties of the data such as the distribution of values and their autocorrelation functions (within 1 year) are not affected by the shuffling procedure, but the statistical dependence between different nodes is diminished. The shuffling method we use here is designed specifically to study the significance of climate network results and is more restrictive compared to conventional surrogate data tests [15–17]. Figure 1(a) depicts the temporal average positive link weights, $\langle W^{+}\rangle$, versus the geographical distances of the links D, for the real and shuffled data in the equatorial Pacific regions (from 2°S to 2°N). High positive average link weight values which exist in the real data but not in the shuffled data are less likely to occur by chance. We thus consider only links that are separated from the shuffled links (indicated by the horizontal dashed lines and vertical arrows in figure 1(a)); in addition, short distanced links (indicated by the vertical dashed line and the horizontal arrow in figure 1(a)) exhibit trivial correlations and are thus ignored (the 'proximity effect' [15]). The probability density function (PDF) of average link weight in this region can be seen in figure B1 in appendix B. We find that significant links with a p-value $p \leqslant 0.02$ include 26.6% of the weighted links in the equatorial Pacific (2°S–2°N), 6.5% for 4°N–7°N, and 11.7% for 4°S–7°S.

One of the main characteristics of equatorial Kelvin waves is their phase speed (which is equal to their group velocity since these waves are non-dispersive)—in the following we use the links' statistics to estimate this

velocity. We note that the long-Rossby waves we discuss below are also non-dispersive and thus their phase speed is equal to their group velocity. Assuming that the delay time τ^* is a good estimator for a dynamical interaction time between two nodes [26], the phase velocities can be estimated by dividing the geographical distance D between the nodes by the delay time τ^*, i.e., $v \approx D/\tau^*$. The PDF of phase speeds (of links with $D \geqslant 500$ km and $p \leqslant 0.02$) is shown in figure 1(c). For the equatorial Pacific, the phase speed is positive (eastward) and peaks around 3 m s^{-1}, in agreement with the value and direction of Kelvin waves [8, 27].

After relating the network links with the equatorial Kelvin waves, the network properties can be used to study the wave dynamics. We found the topological properties of the climate network in equatorial Pacific region show distinct behavior during El-Niño and normal times. The climate network considered above is directed—positive and negative τ^* indicating eastward and westward propagation respectively. We distinguish between a link that is pointing towards a node, or away from the node; the former/ latter is related to the total link weight pointing to/ from a specific node and is referred to below as weighted 'in'/ 'out'-degree. Figures 1(b) and (d) depict the 'in' and 'out' weighted degree versus longitude, averaging over all the latitudes from 2°S to 2°N during El-Niño and normal times, respectively. First, we find that the 'out'-weighted degree is peaked around 170°E at the equator with a much more pronounced peak during El-Niño, which indicates enhanced Kelvin waves activity, consistent with previous, more conventional, analysis [6]. Indeed, stronger Kelvin wave activity during El-Niño around 170°E was associated with strong WWBs [28], which is enhanced wind activity that underlies the generation of equatorial Kelvin waves. Another important method to track the origin of waves in the ocean is the adjoint methods; see, e.g., [29, 30]. Second, there is a peak in the 'in'-weighted degree curve at ∼220°E during both El-Niño and normal times, where for El-Niño times the 'in' degree curve is high all the way to the coast of South America while during normal times the 'in'-degree curve decays for longitudes larger than ∼220°E. We interpret this decay as strong dissipation of the Kelvin waves, and our results suggest that the dissipation of Kelvin waves is much weaker during El-Niño.

The attenuation of the Kelvin waves to the east of ∼220°E during El-Niño was implied based on wave packets (found using Hovmöller diagrams) using model data (oceanic general circulation model simulations) [22, 31]. This attenuation may be attributed to several mechanisms, including the strong vertical current shear during La-Niña, strong wind at ∼220°E [31], scattering of waves, and partial reflection of Kelvin waves into Rossby waves [22]. Here, we use the climate network approach to quantify the waves properties in a statistical and consistent way, all using observational data. Note that our climate network based technique developed here is robust to the filtering procedure, compared with conventional studies (see [5] as one example); i.e., different range of filtering frequencies yield similar results (see figure C1 in appendix C).

3.2. Off-equatorial Pacific

We next apply the climate network methodology to the northern and southern tropical Pacific to study Rossby (and other) tropical waves, respectively. The statistical properties of positive links in the climate networks in the northern tropical Pacific (4°N–7°N) and southern tropical Pacific (4°S–7°S), are shown in figure 2. The phase speed that is calculated based on links above significance level ($p \leqslant 0.02$ and $D \geqslant 500$ km) is negative (westward) and their PDF peaks around 0.5 m s^{-1} and 0.6 m s^{-1} respectively (figures 2(c) and (d)), in general agreement with the phase velocity of TIWs and Rossby waves [7, 8, 32–35]. The structure of link weight versus distance is different for the northern and southern tropical Pacific (figures 2(a) and (b)); see [7] and figures D1 and D2 in appendix D. Network analysis based on northern tropical Pacific is presented in figure 3. The westward propagation of waves is evident during both normal and El-Niño times, with most of the wave activity concentrated between 200°E and 250°E (see also [7]). Evidently, extra-tropical waves are less pronounced during El-Niño times (figure 3). The enhanced wave activity during normal times can be associated with the TIW. The reason is that the TIW are easily recognizable in the Pacific, extending westward from South America. They are stronger during normal times, and may disappear during strong El-Niño [34]. The characteristic phase speed, locations and wave activity during El-Niño of TIW indeed fits the network observations [34].

The TIW are not directly related to the theory of El-Niño even though they are possible sources of random perturbations that affect both the mean state and interannual climate variations. Therefore, we filter them out by employing a sixty days low-pass filter on the SSH data as their characteristic period is about 30 d, which is much smaller than the period of Rossby waves [35]. After this filtering, we reconstruct the climate network and calculate the corresponding wave characteristics (see figures E1 and E2 in appendix E). According to these results, we relate this 'filtered' climate network with Rossby waves, which play an essential role in the self-sustained El-Niño dynamics. Figure 4 depicts the weighted degree at 4°N during El-Niño and normal times. The Rossby waves signal, represented here by the weighted degree of the climate network, is only clearly observed mainly to the west of ∼ 240°E (120°W) (see figure 4), although some of Rossby waves close to the eastern boundary (∼280°E) are the reflection of Kelvin waves. Note that Rossby waves are more pronounced during El-Niño times: Around the date line (180°E) there is a peak in the weighted degree, which is associated to the strong WWBs activity in this region (the same mechanism that generates equatorial Kelvin waves). The delayed oscillator theory suggests that the oceanic Rossby and Kelvin waves

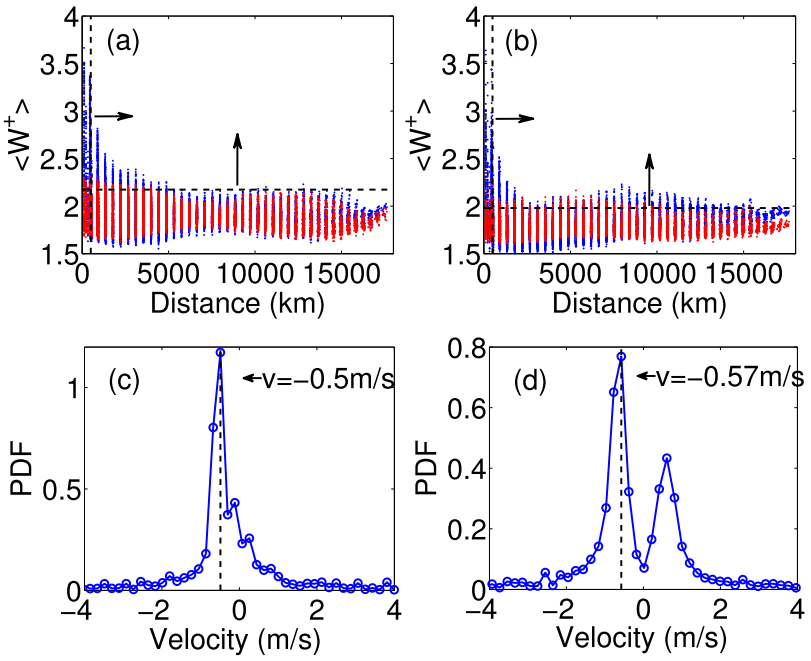

Figure 2. The temporal average link weight $\langle W^{+}\rangle$ versus geographical distance D in (a) the northern tropical Pacific (4°N–7°N) and (b) the southern tropical Pacific (7°S–4°S). The PDF of phase velocity in (c) the northern tropical Pacific and (d) the southern tropical Pacific.

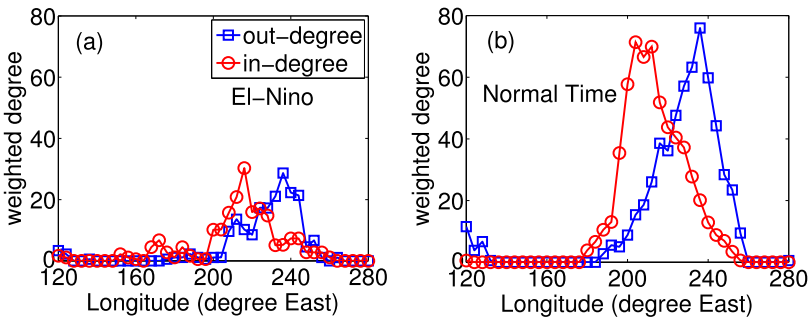

Figure 3. The out- (blue squares) and in- (red circles) weighted degree of nodes in the climate network from 4°N to 7°N during (a) El-Niño times and (b) normal times.

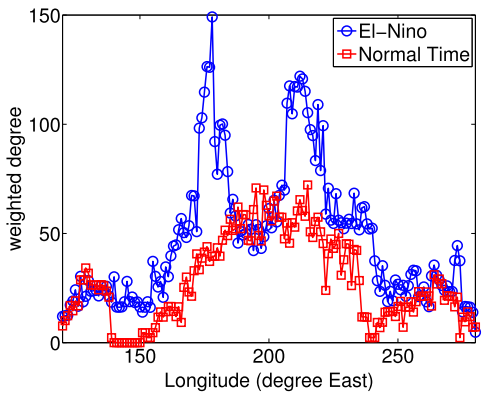

Figure 4. The weighted degree in 4°N for El-Niño (blue circles) and normal (red boxes) times.

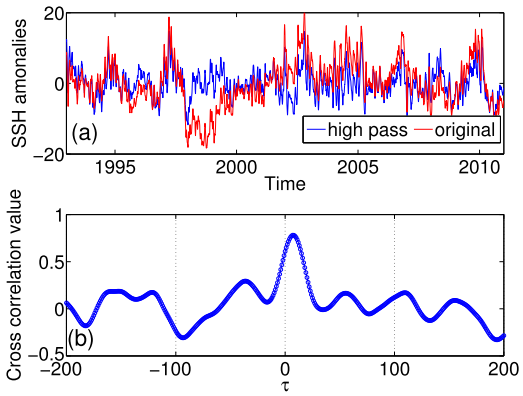

Figure A1. (a) An example for SSH original (red) and high-pass filtered (blue) time series at (0°, 180°E). (b) The cross-correlation function between the high-pass filtered time series of 1993 shown in (a) and time series from (0°, 160°W).

forced by changes in atmospheric wind stress in the central Pacific (the same location as our results) provides mechanism for the ENSO cycle [2]. More specifically, fast eastward downwelling (warm temperature) Kelvin waves and slow westward downwelling Rossby waves are generated in the central Pacific as a results of wind forcing. The Kelvin waves warm the eastern Pacific. At the same time the Rossby waves collide with the western boundary of the Pacific and are reflected as upwelling (cold temperature) Kelvin waves which propagate to the east, to terminate the initial warming. Our results regarding the propagation and reflection effect near the boundaries (figures 1(b), (d) and 4) support the delayed oscillator mechanism. In addition, there is another peak in the weighted degree distribution, between ∼200°E and ∼230°E. Evidently, there are strong fluctuations of wind stress curl in the same region. It has been shown that the spatial distribution of wind stress curl variability is very similar to that of the fully filtered SSH (see figures 2 and 6 in [7]). Moreover, the similarity between the temporal characteristics of SSH and wind stress curl shown in [7] suggests that local wind activities near 140°W generate oceanic Rossby waves. Thus, our results also support the recent suggestion that the enhanced wind-stress curl can be related to the Rossby wave activity. At last, we also calculated the standard deiations of the weighted degree shown in figure 4 and found that the normal and El-Niño curves are well separated in the vicinity of the two maxima.

4. Summary

In summary, we construct and analyze the climate network of the tropical Pacific ocean based on daily satellite SSH data (altimetry). We find that the most dominant long distance links in the network share the same characteristics (i.e. speed and direction) as equatorial Kelvin, Rossby waves, and TIWs, indicating that climate network approach is useful to capture oceanic wave activity. This conclusion is further strengthened by the observation that the location of hubs in network coincide with the location of initiation regions of equatorial oceanic waves. Importantly, a simple network property, i.e. node weighted degree, can be used to quantify the wave activity directly from observational data, with robust features that are not sensitive to the filtering procedures compared with conventional studies. The climate network properties indicate distinct features of wave dynamics during El-Niño and normal times, such as the pronounced equatorial Kelvin and Rossby waves, and suppressed TIW during El-Niño. In addition, the dissipation of Kelvin waves are much weaker during El-Niño. This newly developed methodology based on long-term observational data (18 years) could serve as a quantitative tool to improve our understanding of the underlying wave dynamics of El-Niño, especially regarding the location of their initiation and the dissipation. Finally, our results may also be linked to Indian monsoon activities through teleconnections between El-Niño and Indian monsoon activities and how the oceanic wave activities behave during monsoon seasons versus non-monsoon seasons need to be unravelled in future studies [36].

Recent studies have demonstrated the ability of climate network based-techniques to predict El-Niño events [17, 37]. This technique is based on atmospheric data above the sea surface, although as shown here the ocean plays a central role in El-Niño phenomenon. Based on the present study we conjecture that the inclusion of oceanic data into network analysis will improve the prediction power of network techniques.

Acknowledgments

The authors would like to acknowledge the support of the LINC project (no. 289447) funded by the EC's Marie-Curie ITN program (FP7-PEOPLE-2011-ITN), Multiplex (No. 317532) EU projects, the DFG and the Israel

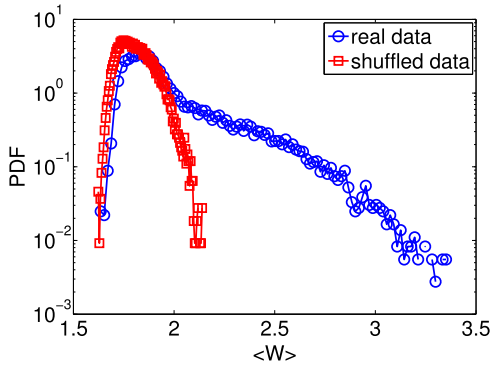

Figure B1. The PDF of the average link weight in the equatorial Pacific region, of real (blue) and shuffled (red) data.

Science Foundation for financial support. We thank D Zhou for helpful discussions. YW thanks the China Scholarship Council for partial support. The Ssalto/Duacs altimeter products were produced and distributed by the Copernicus Marine and Environment Monitoring Service (CMEMS).

Appendix A. SSH anomalies and the cross correlation function

We first consider an example of SSH anomaly time series at (0°, 180°E). To exclude the very low frequencies that are associated with tropical Pacific dynamics [7] we perform a two years high-pass filter (see main text). The original and high-pass filtered SSH time series are shown in figure A1(a). The cross-correlation function of high-pass filtered time series between two sites (0°, 180°E) and (0°, 200°E) (2000 kilometers away from each other), is shown in figure A1(b). The peak of the cross-correlation function is ∼0.9 ($W \sim 3.5$, figure A1(b)) and is significantly higher compared to the background level.

Appendix B. The distribution of mean link weight in the equatorial Pacific

We present in figure B1 the PDF of mean link weights $\langle W \rangle$, from the equatorial Pacific (2°S and 2°N). High mean-link-weight values ($\langle W \rangle \geqslant 2.2$) exist in the PDF of the original data but not in the PDF of the shuffled data. This difference between the PDFs of the real and shuffled data indicates that many significant links exist in the climate network of the equatorial Pacific region.

Appendix C. The Kelvin wave results based on different filtering procedures

In this section, we show that the main results of the equatorial Kelvin waves are not sensitive to filtering procedure (or filtering range). We consider here (i) two-years high pass filter, (ii) one-year high pass filter, and (iii) half a year high pass filter. We focus on the phase speed of the equatorial Kelvin waves. In addition, we analyze the network structure during El Niño and La Niña (the counterpart of El Niño). We concentrate on the 1994, 1997, 2002 and 2004 El Niño events and on 1998–2000, and 2007/2008 La Niña events. The results are shown in figure C1 , where the first, the second and the third rows depicts the results based on two-years, one-year, and half year high-pass filter respectively. Clearly the results are similar indicating that our method is not sensitive to the filtering procedures. The PDF of phase speed (figures C1(c), (f) and (i)) embedded in the climate network has a significant peak at around 3.1 m s^{-1} to the east, which is consistent with the Kelvin wave phase speed. Moreover, the network structure (or mean weighted degree) show the same picture (figures C1(a), (b), (d), (e), (g), (h)): (i) the out-weighted degree (blue squares) is more pronounced during El Niño at around 180°E; (ii) the in-weighted (red circles) degree during El Niño decays around ∼140°W–120°W; (iii) the decay is faster during La Niña than that during El Niño.

Appendix D. The differences between the networks of the northern and southern tropical Pacific

As shown in figure 2 of the main text, there are differences between the network characteristics of the northern and southern tropical Pacific. Specifically, the link weight distribution decays faster with distance in the south compare to the north (see figure 2 of the main text). The standard deviation of delays std(τ^*) for strong positive links ($p \leqslant 0.02$) is shown in figure D1 . It is implied that in the southern region (figure D1(b)) there is a large group of long-distance

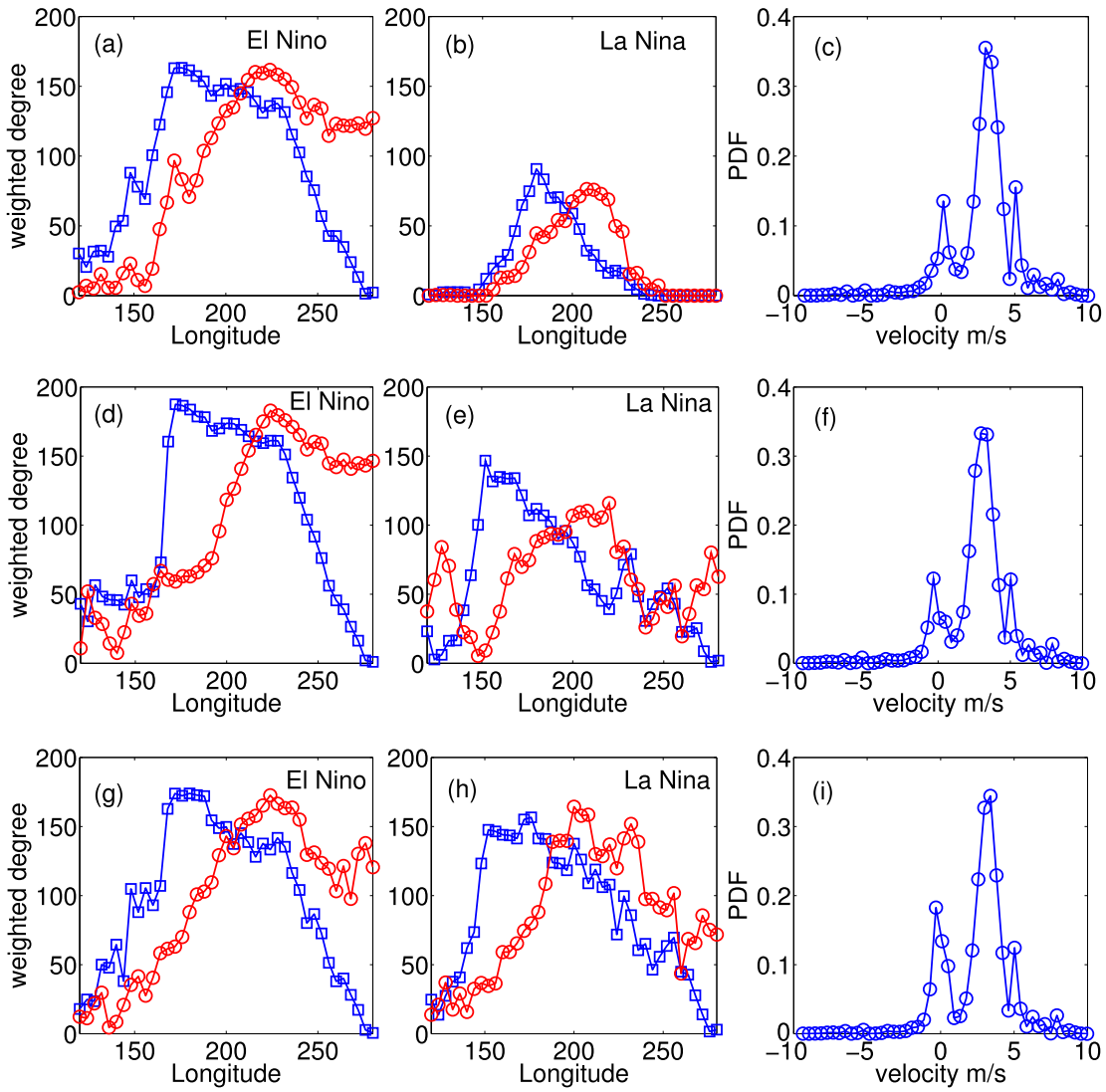

Figure C1. The network structural properties under different filtering schemes. The first, second, and third row of the figure shows the results using two years, one year, and half a year high pass filters, respectively. The first and second columns of the figure show the out-weighted (blue squares) and in-weighted (red circles) at different longitude during El Niño and La Niña, respectively. The third row is the PDF of the phase speed calculated based on the climate network.

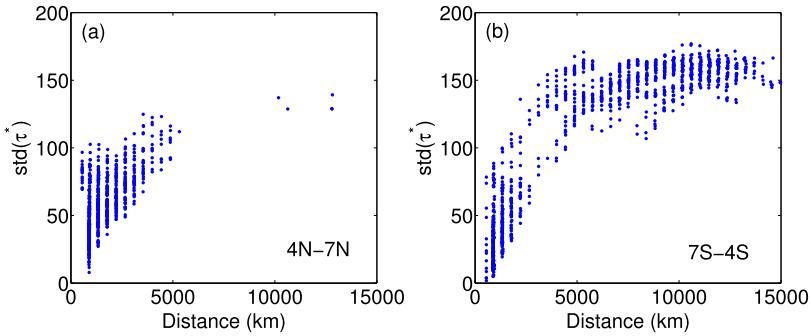

Figure D1. The standard deviation of delays for strong positive links as a function of geographical distance ($p \leqslant 0.02$ and $D \geqslant 500$ km) for the (a) northern and (b) southern tropical Pacific.

links (longer than 4000 km) with large std(τ^*) values (around 150 d); such links are, most probably, reminiscent of noise [38]. These links do not exist in the northern region (figure D1(a)). Hence, to exclude such 'noisy' links, we restrict ourselves to distances smaller than 4000 km, in both regions. Figure D2 depicts the PDF of delays of these ('non-noisy') positive links, both in the northern and southern tropical Pacific. For the northern part the PDF is uni-modal while in the southern part the PDF is bi-modal with two comparable maxima at $\tau^* = -15$ and $\tau^* = 0$ d.

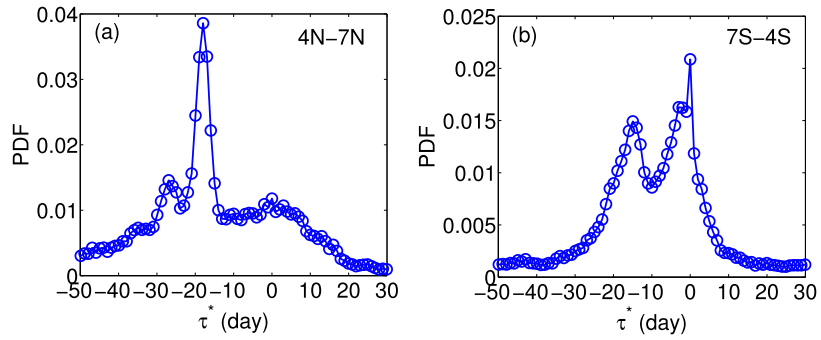

Figure D2. The PDF of delays for positive links with $p \leqslant 0.02$ and 500 km $\leqslant D \leqslant$ 4000 km, for the (a) northern and (b) southern tropical Pacific.

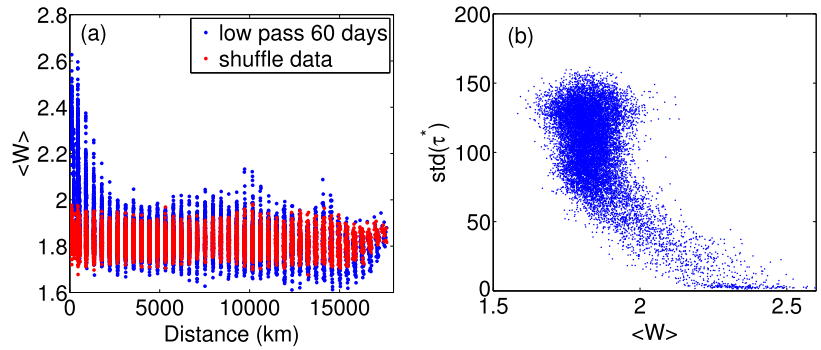

Figure E1. The statistical properties of links in northern tropical Pacific (4°N–7°N). (a) Mean link weight $\langle W \rangle$ versus distance of links (after applying sixty days low-pass filter). (b) (std(τ^*)) as a function of average link weight, $\langle W \rangle$.

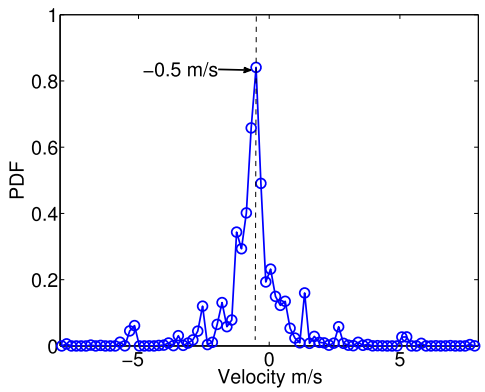

Figure E2. The phase speed of Rossby waves in the northern Pacific (4°N–7°N), based on positive links with $p \leqslant 0.02$ and 500 km $\leqslant D \leqslant$ 4000 km, after applying 60 d low-pass filter.

The peak at −15 d (figure D2(b)) reflects westward wave propagation. We currently cannot explain the peak at $\tau^* = 0$.

Appendix E. The representation of Rossby waves in the climate network

As discussed in the main text, TIWs have similar phase speed as Rossby waves, making it difficult to study Rossby waves. We thus filter out the TIW frequency range (with an average period of ∼30 d [35]) by employing a sixty days low-pass filter on the SSH records. The dependency of link weights on distance D and a scatter plot of link weights and std(τ^*) for the filtered data is shown in figure E1. As explain in the main text, we shuffled the data to

estimate the threshold, and consider links with $p \leqslant 0.02$. To rule out the 'proximity' effect and to exclude links with high std(τ^*) we also restrict ourselves to distances 500 km $\leqslant d \leqslant$ 4000 km. The PDF of phase speeds obtained from these links is shown in figure E2, having a peak around $\tau = -0.5$ m s^{-1}, consistent with the phase speed of oceanic Rossby waves in this region [7].

References

[1] Turner J 2004 The El Niño-southern oscillation and Antarctica *Int. J. Climatol.* **24** 1
[2] Clarke A J 2008 *An Introduction to the Dynamics of El Niño the Southern Oscillation* (London: Elsevier)
[3] Cane M A and Sarachik E S 2010 *The El Niño-Southern Oscillation Phenomenon* (Cambridge: Cambridge University Press)
[4] Gill A E 1982 *Atmosphere-Ocean Dynamics* (New York: Academic)
[5] Roundy P E and Kiladis G N 2006 Observed relationships between oceanic Kelvin waves and atmospheric forcing *J. Clim.* **19** 5253–72
[6] McPhaden M J and Yu X 1999 Equatorial waves and the 1997–98 El Niño *Geophys. Res. Lett.* **26** 2961–4
[7] Chelton D B, Schlax M G, Lyman J M and Johnson G C 2003 Equatorially trapped Rossby waves in the presence of meridionally sheared baroclinic flow in the Pacific ocean *Prog. Oceanogr.* **56** 323–80
[8] Wakata Y 2007 Frequency-wavenumber spectra of equatorial waves detected from satellite altimeter data *J. Oceanogr.* **63** 483–90
[9] Delcroix T, Boulanger J-P, Masia F and Menkes C 1994 Geosat-derived sea level and surface current anomalies in the equatorial Pacific during the 1986–1989 El Niño and La Niña *J. Geophys. Res.* **99** 25093–107
[10] Tsonis A A and Swanson K L 2008 Topology and predictability of El Niño and La Niña networks *Phys. Rev. Lett.* **100** 228502
[11] Newman M E J 2010 *Networks: An Introduction* (New York: Oxford University Press)
[12] Cohen R and Havlin S 2010 *Complex Networks: Structure, Robustness and Function* (Cambridge: Cambridge University Press)
[13] Yamasaki K, Gozolchiani A and Havlin S 2008 Climate networks around the globe are significantly affected by El Niño *Phys. Rev. Lett.* **100** 228501
[14] Donges J F, Zou Y, Marwan N and Kurths J 2009 The backbone of the climate network *Europhys. Lett.* **87** 48007
[15] Wang Y, Gozolchiani A, Ashkenazy Y, Berezin Y, Guez O and Havlin S 2013 Dominant imprint of Rossby waves in the climate network *Phys. Rev. Lett.* **111** 138501
[16] Berezin Y, Gozolchiani A, Guez O and Havlin S 2012 Stability of climate networks with time *Sci. Rep.* **2** 666
[17] Ludescher J, Gozolchiani A, Bogachev M, Bunde A, Havlin S and Schellnhuber H J 2013 Improved El Niño forecasting by cooperativity detection *Proc. Natl Acad. Sci.* **110** 11742
[18] Gozolchiani A, Yamasaki K and Havlin S 2011 The emergence of El-Niño as an autonomous component in the climate network *Phys. Rev. Lett.* **107** 148501
[19] Feng Q and Dijkstra H 2014 Are north Atlantic multidecadal SST anomalies westward propagating *Geophys. Res. Lett.* **41** 541–6
[20] Ser-Giacomi E, Rossi V, Lpez C and Hernndez-Garca E 2015 Flow networks: a characterization of geophysical fluid transport *Chaos* **25** 036404
[21] Feng Q Y, Viebahn J P and Dijkstra H A 2014 Deep ocean early warning signals of an Atlantic MOC collapse *Geophys. Res. Lett.* **41** 6009–15
[22] Mosquera-Vsquez K, Dewitte B and Illig S 2014 The central Pacific El Niño intraseasonal Kelvin wave *J. Geophys. Res.: Oceans* **119** 6605–21
[23] Runge J, Petoukhov V, Donges J F, Hlinka J, Jajcay N, Vejmelka M, Hartman D, Marwan N, Palus M and Kurths J 2015 Identifying causal gateways and mediators in complex spatio-temporal systems *Nat. Commun.* **6** 8502
[24] Runge J, Petoukhov V and Kurths J 2014 Quantifying the strength and delay of climatic interactions: the ambiguities of cross correlation and a novel measure based on graphical models *J. Clim.* **27** 720–39
[25] Zhou D, Gozolchiani A, Ashkenazy Y and Havlin S 2015 Teleconnection paths via climate network direct link detection *Phys. Rev. Lett.* **115** 268501
[26] Cimponeriu L, Rosenblum M and Pikovsky A 2004 Estimation of delay in coupling from time series *Phys. Rev.* E **70** 046213
[27] Toshiaki S, Roundy P and Kiladis G 2008 Variability of intraseasonal Kelvin waves in the equatorial Pacific ocean *J. Phys. Oceanogr.* **38** 921–44
[28] Eisenman I, Yu L and Tziperman E 2005 Westerly wind bursts: ENSO's tail rather than the Dog? *J. Clim.* **18** 5224–38
[29] Heimbach P, Wunsch C, Ponte R M, Forget G, Hill C and Utke J 2011 *Deep-Sea Res.* II **58** 1858–79
[30] Galanti E and Tziperman E 2003 A midlatitude ENSO teleconnection mechanism via baroclinically unstable long Rossby waves *J. Phys. Oceanogr.* **33** 1877–88
[31] Benestad R E, Sutton R T and Anderson D L T 2002 The Effect of El Niño on Intraseasonal Kelvin Waves *Q. J. R. Meteorol. Soc.* **128** 1277–91
[32] Kessler W S 1990 Observations of long Rossby waves in the northern tropical pacific *J. Geophys. Res.* **95** 5183–217
[33] Chelton D B and Schlax M G 1996 Global observation of oceanic Rossby waves *Science* **272** 234–8
[34] Willett C S, Leben R R and Lavín M F 2006 Eddies and tropical instability waves in the eastern tropical pacific: a review *Prog. Oceanogr.* **69** 218–38
[35] Lyman J M, Chelton D B, Deszoeke R A and Samelson R M 2005 Tropical instability waves as a resonance between equatorial Rossby waves *J. Phys. Oceanogr.* **35** 232–54
[36] Kumar K K, Rajagopalan B, Hoerling M, Bates G and Cane M 2006 Unraveling the mystery of indian monsoon failure during El Niño *Science* **314** 115–9
[37] Ludescher J, Gozolchiani A, Bogachev M I, Bunde A, Havlin S and Schellnhuber H J 2014 Very early warning of next El Niño *Proc. Natl. Acad. Sci. USA* **111** 2064–6
[38] Bashan A, Bartsch R P, Kantelhardt J W, Havlin S and Ivanov P C 2012 Network Physiology reveals relations between network topology and physiological function *Nat. Commun.* **3** 702